ELSEVIER

Materials Science and Engineering A233 (1997) 61–74

MATERIALS SCIENCE & ENGINEERING A

Plastic deformation of zirconia single crystals: a review

Ulrich Messerschmidt *, Dietmar Baither, Bernd Baufeld, Martin Bartsch

Max Planck Institute of Microstructure Physics, Weinberg 2, Halle/Saale, D-06120, Germany

Received 12 September 1996; received in revised form 12 November 1996

Abstract

The high-temperature deformation behaviour of zirconia single crystals stabilised with yttria is reviewed. Cubic or fully stabilised zirconia (FSZ), which is considered the matrix of high-strength partially stabilised zirconia (PSZ), deforms plastically down to 400°C without confining hydrostatic pressure. The relevant deformation behaviour above about 1200°C is characterised by athermal dislocation motion mainly on cube slip planes and diffusion-controlled recovery. Tetragonal polydomain zirconia or t′ zirconia consists of plate-like tetragonal domains alternately stacked to form large colonies. These colonies are arranged in a characteristic way to fill the whole crystal volume. t′ zirconia shows ferroelastic behaviour preceding dislocation plasticity. In tension, a tetragonal single crystal forms containing residual defects. The data available indicate that the coercive stress strongly depends on temperature. In situ straining experiments in a high-voltage electron microscope show an instantaneous switching of the individual tetragonal domains with the domain boundaries moving sidewise through the domains. Dislocations moving after the ferroelastic deformation are strongly bowed. The nature of the pinning agents is not clear yet. PSZ crystals are thought to consist of a cubic matrix and precipitates of the tetragonal phase of a structure similar to that of the colonies in t′ zirconia. Complete dislocations in the cubic matrix moving on cube planes are partial dislocations in two of the three tetragonal variants of the precipitates. They have then to produce a stacking fault or antiphase boundary like defect. The strong age-hardening and overageing experimentally observed can be explained by a decreasing width of the matrix channels between the precipitates and an increasing width of the domains within the colonies. Recent in situ studies in a high-voltage electron microscope have shown that the precipitates in PSZ may undergo ferroelastic deformation, too. Besides, in a number of cases the matrix of PSZ crystals turned out to be tetragonal rather than cubic. Thus, the formation of a tetragonal single crystal containing residual defects as during the ferroelastic deformation in t′ zirconia should affect the subsequent dislocation plasticity. The stacking fault or antiphase boundary like defects have experimentally been observed on {110} planes, however, not on the usual {100} slip planes. Thus, in spite of numerous experimental results a number of questions are still open particularly concerning the plastic deformation of PSZ crystals. © 1997 Elsevier Science S.A.

Keywords: Zirconia; Plastic deformation; Yttria; Dislocations; Precipitation hardening; Ferroelastic deformation

1. Introduction

Zirconia may serve as a constituent of materials with attractive properties for structural applications in a wide range of temperatures. The tetragonal-to-monoclinic transformation is used for designing tough materials around ambient temperature [1,2]. At high temperatures, partially stabilised zirconia (PSZ) may have a very high yield stress due to precipitation hardening [3–6]. In addition, ferroelastic deformation observed in so-called t′ zirconia may contribute to a high toughness at high temperatures [7–9]. The present paper reviews the literature on the deformation mechanisms in different yttria-stabilised zirconia single crystals and describes a few experimental results of the authors not yet published. The structure of yttria-stabilised zirconia crystals is briefly outlined in Section 2. As the matrix of partially stabilised zirconia is supposed to consist of cubic zirconia, its deformation processes are reviewed in Section 3. The precipitates in PSZ have a tetragonal crystal structure. t′ zirconia is a single phase tetragonal material. Its deformation processes described in Section 4 may help understand the deformation behaviour of the precipitates in PSZ, which is finally treated in Section 5. Section 6 gives conclusions and raises some open questions.

* Corresponding author. Tel.: +49 345 5582927; fax: +49 345 5511223.

PII S0921-5093(97)00050-6

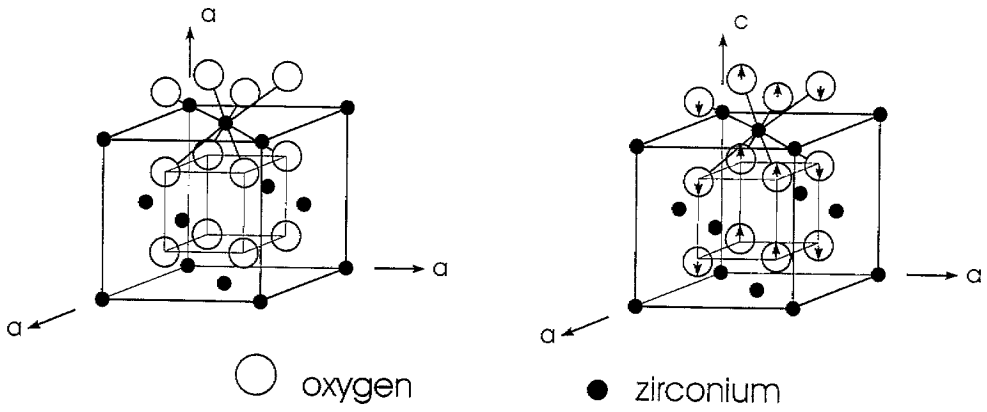

Fig. 1. Crystal structure of zirconia.

2. Structure of yttria-stabilised zirconia crystals

For an early review of the structure and microstructure of the ZrO_2-Y_2O_3 materials, see [10]. Pure zirconia has the CaF_2 structure at temperatures above about 2400°C. As the left side of Fig. 1 shows, zirconium ions occupy the sites in a face-centered cubic unit cell, while oxygen ions are situated in 1/4 ⟨111⟩ and equivalent positions. Below 2400°C, ZrO_2 undergoes a transformation to the tetragonal phase. In addition to a small elongation of about 2% in direction of the c-axis, rows of oxygen ions are shifted in upward or downward directions as indicated on the right of Fig. 1.

These high-temperature phases can be stabilised down to low temperatures by adding aliovalent cations. According to the ZrO_2-Y_2O_3 phase diagram [11,12], the cubic phase is stabilised at Y_2O_3 concentrations higher than about 8–10 mol% (fully stabilised zirconia, FSZ). At lower yttria concentrations, yttria-lean precipitates form in an yttria-rich matrix (partially stablisied zirconia, PSZ). This diffusion-controlled precipitation reaction proceeds very slowly owing to the sluggish cation diffusion requiring long times to achieve the equilibrium concentration of the precipitated tetragonal phase. A variety of microstructures can form depending on the yttria concentration, annealing temperature and duration. These processes are described in detail in [13]. The diffusive transformation cannot take place during quenching from the cubic phase field. The crystals then undergo a displacive phase transformation to a metastable tetragonal material of uniform yttria concentration, the so-called tetragonal polydomain zirconia or t′ zirconia.

3. Deformation of cubic zirconia

Cubic zirconia may constitute the matrix of two-phase materials. Its deformation behaviour has been extensively studied, particularly at a temperature of 1400°C, and higher (e.g. [14–17]). Recently, it was reported that it was possible to deform the material down to 400°C without confining hydrostatic pressure [18,19]. The deformation behaviour of cubic zirconia is reviewed in [20] and is therefore only briefly described here.

The Burgers vectors are of type 1/2 ⟨110⟩. Slip occurs mainly on {100} planes. Most experiments are carried out with a ⟨211⟩ compression or tensile axis, favouring single slip on one cube system. At high temperatures, {110} and {111} planes may be activated as secondary slip planes. These planes are also activated if cube slip is suppressed by a ⟨100⟩ deformation axis. Fig. 2 outlines the deformation behaviour of cubic zirconia at different temperatures. All experiments include also stress relaxation and strain rate cycling tests. The temperature range best understood is the range

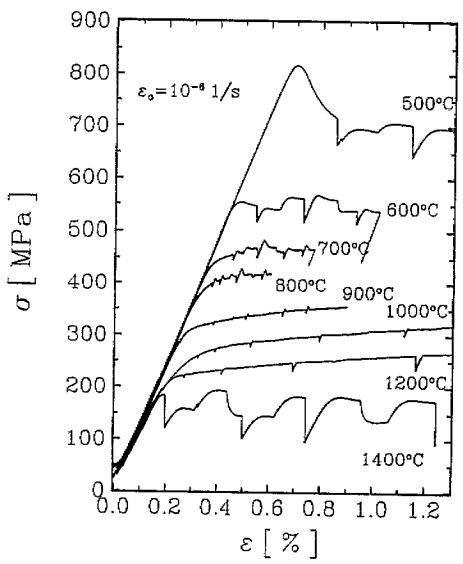

Fig. 2. Stress-strain curves of ZrO_2-11 mol% Y_2O_3 at different temperatures. After [19].

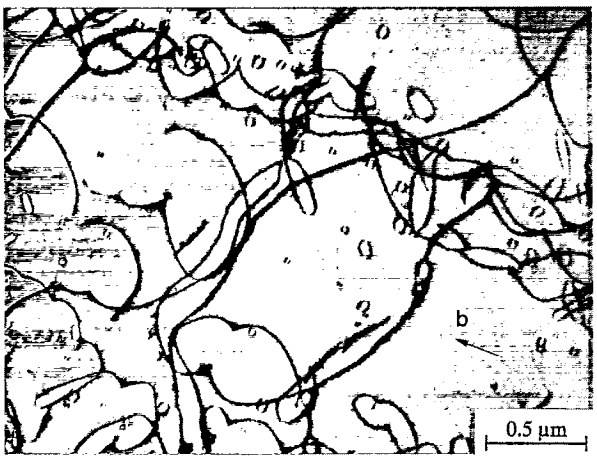

Fig. 3. Dislocation structure of ZrO_2-11 mol% Y_2O_3 deformed at 1000°C along ⟨112⟩. After [19].

around 1150°C, where slip preferentially occurs on a cube plane and the strain rate sensitivity $I = d\sigma/d \ln \dot{\varepsilon}$ is very small (about 1 MPa). Here, σ is the flow stress and $\dot{\varepsilon}$ is the plastic strain rate. Accordingly, the deformation should be controlled by athermal processes. This means that the energy necessary to surmount barriers to dislocation motion is so high that the major part of it has to be supplied by work done by the external stress rather than by thermal activation. Fig. 3 shows the deformation microstructure, which consists of bundles of parallel dislocations of opposite sign. They are the sources of the long-range stresses which represent the barriers to dislocation motion. Bowing out between large jogs, the dislocations are of curved shape. In addition, many dislocation loops are formed during deformation. In situ straining experiments in a high-voltage electron microscope (HVEM) [21] have revealed a very jerky dislocation motion, usually over distances similar as or larger than those between the dislocations. This confirms the athermal nature of the deformation. As discussed in [20], the flow stress can semiquantitatively be understood by the superposition of the long-range interaction between parallel dislocations (Taylor hardening) and the back stress of the bowed-out dislocations. Dislocation velocities were measured between 1100 and 1450°C by the stress pulse etching technique [22]. Particularly at the low temperature side, these measurements were carried out at low stresses resulting in dislocation velocities which are many orders of magnitude smaller than those of the macroscopic deformation tests described above. The different dislocation behaviour in the etching study and in macroscopic tests is discussed in more detail in [21]. Slip on non-cube systems observed during special in situ straining experiments at 1150°C [21] was viscous, indicating the action of a lattice friction mechanism on non-cube systems at this relatively high temperature. The yield stress along a ⟨100⟩ compression axis is about twice of that along ⟨112⟩.

As shown in Fig. 2, the yield stress of cubic zirconia rises very strongly with decreasing temperature. Down to 400°C, the strain rate sensitivity increases by about two orders of magnitude, indicating the operation of thermally activated processes. These results can be explained in accordance with the microstructural observations by the pinning of dislocations by either small precipitates or jogs [18], and by the Peierls mechanism at very low temperatures [20]. This temperature range is not further discussed here since it is not important for the high-temperature deformation of two-phase zirconia materials.

As qualitatively evidenced by the strain rate cycling and stress relaxation experiments in the deformation curve recorded at 1400°C in Fig. 2, the strain rate sensitivity is also high at high temperatures. Details of this behaviour are shown in the stress relaxation curves of Fig. 4. It was already shown in [23] that particularly for small strains and high strain rates (curve marked by □) the relaxation starts with a steep slope corresponding to a low strain rate sensitivity, as in the athermal range at lower temperatures. After a sharp knee the relaxation curve turns to the usual shape with a high strain rate sensitivity. These shapes can be explained by a superposition of dislocation kinetics with a low strain rate sensititvity, and by recovery taking place during deformation [24].

The dislocation structure of specimens deformed at 1400°C or higher temperatures depends sensitively on the unloading and cooling treatment after the high-temperature deformation. Fig. 5 compares the structure of a specimen cooled in the unloaded condition with that of a specimen cooled under full load down to about

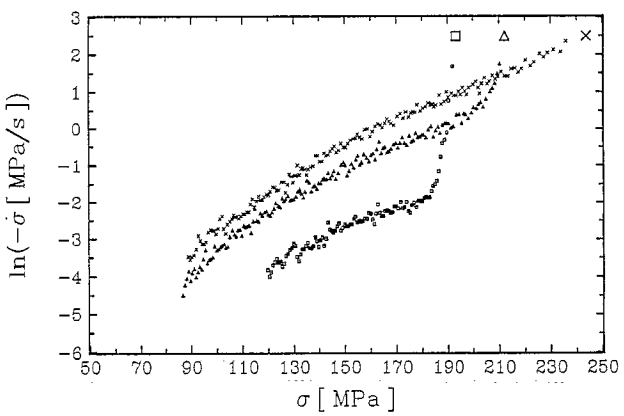

Fig. 4. Stress relaxation curves of ZrO_2-11 mol% Y_2O_3 at 1400°C and a strain rate of 10^{-4} s^{-1}. After [19].

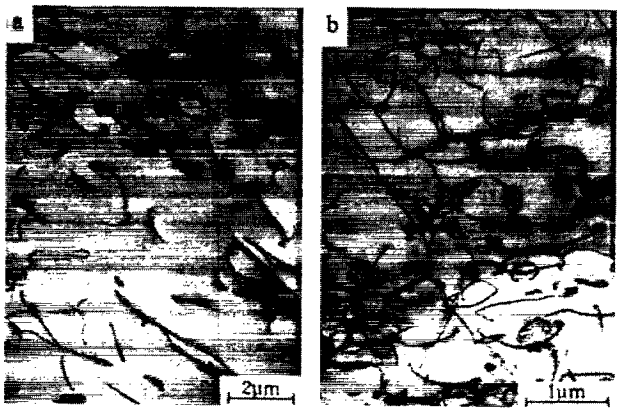

Fig. 5. Comparison between dislocation structures in ZrO_2-11 mol% Y_2O_3 produced by plastic deformation of about 2.5% in $[\bar{1}\,1\,\bar{2}]$ direction at 1400°C. $(\bar{1}\,11)$ foil plane. (a) After cooling without load, (b) after cooling under load. Note the different magnifications in (a) and (b). After [20].

900°C. The differences in the shape of dislocations and particularly in the total dislocation density are obvious. This suggests that dislocation densities usually observed in post mortem specimens do not represent the state during deformation. This is a further indication that recovery plays an important role in the deformation of zirconia at high temperatures. The microstructure consists of weakly bent dislocations on the primary cube system and on secondary (mostly also cube) systems. Junctions are sometimes formed by reactions between primary and secondary dislocations. Some dislocations contain jogs. The junctions and the jogs are the pinning centres for the dislocation bowing. Some dislocation loops and dipoles are also imaged. Neither the junctions nor the jogs or loops or dipoles contribute essentially to the flow stress [20]. The dislocation motion on the cube slip planes is most probably of an athermal nature as in the athermal temperature range. The flow stress is controlled by the interplay between work-hardening by long-range dislocation interactions and by recovery taking place during deformation. The latter is governed by cation diffusion, which depends on the yttria concentration [25]. This explains the influence of the yttria content on the high-temperature yield stress, observed experimentally (e.g. [23]).

In summarising this section it may be stated that dislocations in cubic zirconia are most probably very mobile on cube planes at temperatures above about 1100°C. The yield stress of crystals containing about 10 mol% yttria is about 190 MPa at 1400°C. It arises from long-range dislocation interactions. A relatively high strain rate sensitivity of the flow stress at low strain rates originates from recovery occurring during deformation.

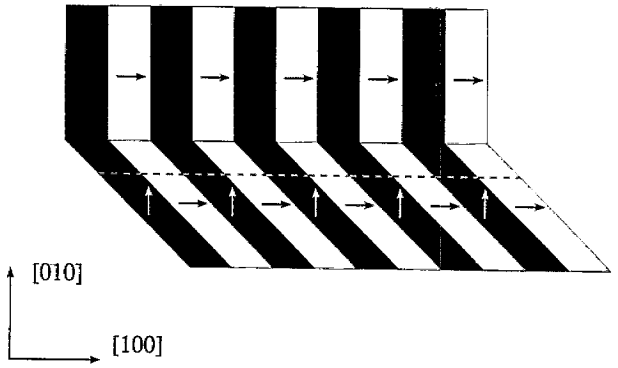

Fig. 6. Tetragonal domains of different orientation of their c-axes forming colonies

4. Deformation of t′ zirconia

As mentioned in Section 2, t′ zirconia is a metastable tetragonal phase of low yttria content, obtained by a diffusionless phase transformation during quenching from the cubic phase field. Its microstructure consists of individual domains with their c-axes in different orientations. The tetragonality amounts to about 1%. The domains are denoted by t_1, t_2 and t_3 depending on their c-axes being parallel to either the x, y or z-axis of the pseudocubic lattice. Domains of alternating c-axes are stacked to form colonies (e.g. [10]) as outlined in the schematic picture of Fig. 6. The domain boundaries are the {101} twin planes. Fig. 7 shows the typical domain structure. The arrangement of the colonies filling the whole volume of the crystals was derived from analysing relatively thick specimens in an HVEM [26]. According to this study, the colonies grow preferentially in ⟨111⟩ directions. Owing to the small deviation from the orthogonality of the c-axes, always three colonies of equal growth direction, consisting of different combinations of the t_1, t_2 and t_3 domains, form

Fig. 7. Microstructure of t′ zirconia.

Fig. 8. Microstructure of t′ zirconia partly transformed by ferroelastic deformation during an in situ straining experiment in an HVEM.

helical arrangements, where the boundaries between the individual colonies are again {101} twin planes. The colonies in t′ zirconia are supposed to have a structure similar to that of the tetragonal precipitates in partially stabilised zirconia.

Under stress, t′ zirconia may undergo ferroelastic deformation [7–9]. During tensile loading along a pseudocubic axis, domains of c-axes different from the loading axis may switch into that type with the c-axis in the tensile direction, forming a tetragonal single crystal. In compression, that type of domains with the c-axis parallel to the compression axis may disappear. Considering the tetragonality of t′ zirconia of about 1%, the maximum strain induced by ferroelastic deformation is about 2/3 of a percent. Recently, the process of domain switching has directly been observed during in situ straining experiments in an HVEM at 1150°C [27–29]. Usually, the switching of individual domains is very fast so that it cannot be resolved by video recording. The transformation arises by a sidewise motion of the transformation front into the domain rather than from the broadening of the domains having their c-axes parallel to the tensile direction. This is shown in Fig. 8, where the transformation front stopped inside the domains. The untransformed areas appear in strong contrast owing to the electron microscopy contrast of the domain boundaries and the orientation differences between the domains. During transformation, a tetragonal single crystal forms so that this contrast disappears, with the transformation front becoming visible. If the transformation starts simultaneously at different points, the individual transformation fronts will meet. A stacking fault in the oxygen sublattice may remain along the meeting area. Frequently, these antiphase boundary-like (APB-like) defects are situated at the former colony boundaries. Similar defects may be created by dislocation motion, which will be discussed in the next section.

Only very few data are available on the macroscopic parameters of the ferroelastic deformation of t′ zirconia. They are summarised in Table 1 together with reference data of cubic and partially stabilized materials. A typical deformation curve is demonstrated in Fig. 9. According to this limited information, the coercive stress for ferroelastic deformation strongly depends on temperature. It is probably higher than the yield stress of cubic zirconia along the ⟨112⟩ single slip orientation for cube slip and of the order of magnitude of slip along ⟨100⟩, which is the orientation of the experiments on ferroelastic deformation, but it is lower than the yield stress of well aged partially stabilized zirconia. In accordance with this, the macroscopic deformation curves [31] as well as the in situ experiments [29] indicate that ferroelastic domain switching precedes macroscopic dislocation plasticity. The two data points on the strain rate sensitivity of the coercive stress are of the same order of magnitude as the values for plasticity in cubic zirconia.

Almost no information is available on the dislocation processes of plastic deformation in t′ zirconia. In untransformed material, dislocations are mostly invisible owing to the strong electron microscope contrast of the domain structure. Dislocations of Burgers vector 1/2 ⟨110⟩ as in cubic zirconia are complete dislocations in the tetragonal structure only if the Burgers vectors lie in the basal plane. Otherwise, they are partial dislocations which should trail a stacking fault in the oxygen sublattice. The contrast of this defect is similar to that of an antiphase boundary. Superdislocations of two dislocations with 1/2 ⟨110⟩ Burgers vectors including the APB-like defects have never been observed. In addition, dislocations crossing a domain boundary should create a dislocation in the boundary if their Burgers vector is not parallel to the boundary in order to fulfill the Burgers vector conservation rule. On the other hand, in tension ferroelastic deformation preceding dislocation plasticity forms a tetragonal single crystal containing a number of antiphase boundary-like defects along the former colony boundaries. The same structure of a tetragonal single crystal was formed in a macroscopic experiment at 1000°C in compression [31]. Fig. 10 shows dislocations (one marked by an arrow) in the transformed area during an in situ straining experiment on t′ zirconia at 1150°C. These dislocations are strongly bowed-out with segment lengths of the order of magnitude of the former domain width rather than of the former colonies. The strong bowing may correspond well to the flow stress but the type of pinning agent is not known.

Table 1
Coercive stress σ_f of ferroelastic deformation of t′ zirconia, yield stress σ_y of cubic (FSZ) and tetragonal (PSZ) zirconia and respective strain rate sensitivities I

T (°C)	t′		FSZ ⟨112⟩		FSZ ⟨100⟩		PSZ	
	σ_f (MPa)	I (MPa)	σ_y (MPa)	I (MPa)	σ_y (MPa)	I (MPa)	σ_y (MPa)	I (MPa)
1400	<300 [8]		190 [19]	2 (kinetic) [23,19] 40 (recovery) [23,19]	200 (2×10^{-5} s^{-1}) [34] 160 (1.3×10^{-5} s^{-1}) [33] ≅310 (10^{-4} s^{-1}) [19] 200 (10^{-6} s^{-1}) [19]	≅40 [19]	550 (peak) [4] 310 (50 h) [31] 160 ⟨102⟩ [35]	4 (50 h) [31]
1150	≅450 [31]	3 [31]	210 [19]	1 [19]	450 [19]	≅40 [19] 16 [19]		
1000	<700 [8] 750 [9] 285 [30] 365 [31]	4 [31]	260 [18]	1 [19]				
600	430 [30]	20 [30]	550 [19]	30 [19]				
20	1650 [32]							

Thus, ferroelastic domain switching in t′ zirconia precedes plastic deformation. The structural change, frequently implying the formation of a tetragonal single crystal containing APB-like defects may significantly affect the plastic deformation. The microprocesses of dislocation plasticity following ferroelastic deformation are almost unknown.

5. Deformation of partially stabilised zirconia

5.1. Microstructure

Partially stabilised zirconia is obtained by ageing the as-received crystals in the two-phase field of tetragonal and cubic zirconia. The kinetics of ageing at 1600°C and the microstructures obtained are described in [13] for three different yttria concentrations. The materials are supposed to consist of yttria-lean tetragonal precipitates in an yttria-rich cubic matrix. Thus, they may behave like composites of the materials described in Sections 3 and 4. Fig. 11 shows the characteristic microstructure. The precipitates resemble the individual colonies in t′ zirconia, i.e. they consist of twinned domains of approximately equal width with alternating directions of the c-axes. The morphology is described in detail in [36]. The individual platelets are slightly shifted with respect to each other resulting in a faceted interface between precipitates and matrix, and in lateral extensions deviating from the low-index directions usually discussed. The precipitates are built from only two of the three tetragonal variants possible. The third may correspond to the original t′ matrix, which is consistent with other observations. However, it is not clear whether it is a general phenomenon, or not. As just mentioned, during annealing at 1600°C precipitation starts from a t′ phase [13]. Particularly at low yttria concentrations, the as-received material already contains small tetragonal precipitates. Their volume fraction f grows to saturation values of 23% in ZrO_2-5.8 mol% Y_2O_3, of 40% in ZrO_2-4.7 mol% Y_2O_3, and of 45% in ZrO_2-3.4 mol% Y_2O_3. Saturation is always reached after 24 h [13]. The length of the precipitates continuously increases, first rapidly and then moderately, reaching 2 μm for the 4.7 mol% crystals after 1000 h. The precipitates have the shape of elongated fibres with a ratio of about 1:4 between width and length. The yttria concentration of the matrix saturates at about 6.2 mol%. As the inset of Fig. 12 indirectly demonstrates for the 4.7 mol% crystal, as the size of the precipitates increases the spacing between the individual domains grows, reaching 150 nm after 150 h annealing at 1600°C.

5.2. Precipitation hardening

The precipitation process is accompanied by substantial hardening, as shown in Fig. 12 for ZrO_2-4.7 mol% Y_2O_3 deformed along ⟨112⟩ [4]. Macroscopic slip traces indicate glide on a cube plane as in cubic zirconia. For a ⟨100⟩ compression axis, however, slip occurs on {110} planes [6]. The yield stress along ⟨112⟩ increases up to 150 h of ageing at 1600°C. Overageing occurs with a decreasing flow stress after longer annealing times. The mechanisms are described in detail in [4–6]. The main argument is that the dislocations of Burgers vectors 1/2 ⟨110⟩ moving in the matrix are partial dislocations in two of the three tetragonal variants of the precipitates as described above for t′ zirconia. Thus, they have to create stacking faults (in the oxygen sublattice), viz. the same defects mentioned in Section 4, which will be discussed below. The creation of these stacking faults or APB-like defects, which is schematically shown in Fig. 13(a), causes a frictional stress

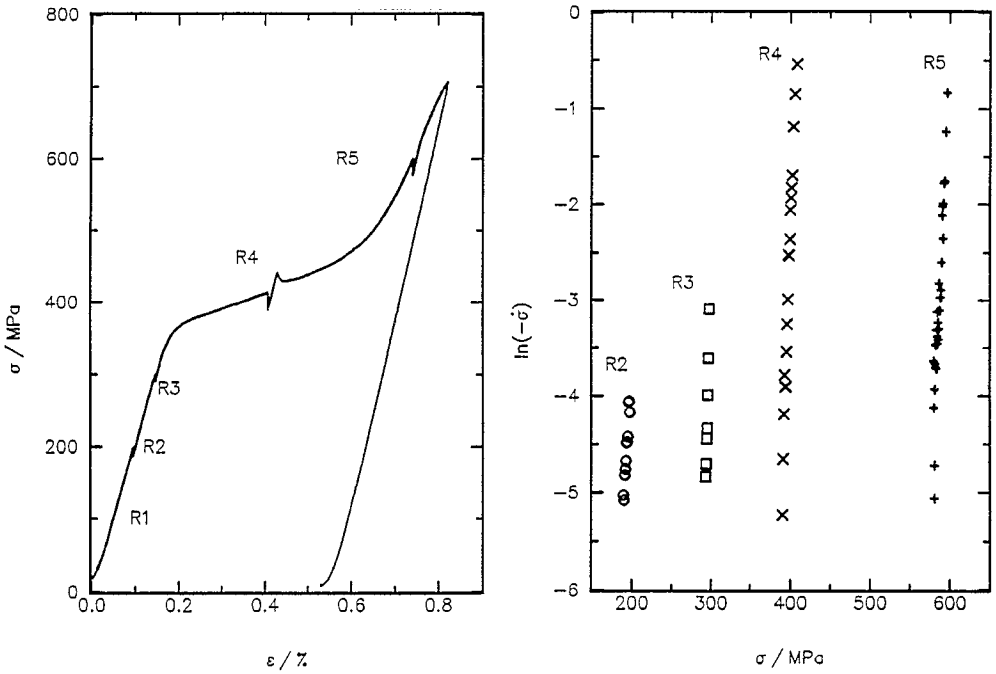

Fig. 9. Stress-strain curve and stress relaxation curves R2 to R5 of t′ ZrO_2-3 mol% Y_2O_3 deformed with $\dot{\varepsilon} = 6 \times 10^{-6}\ s^{-1}$ at 1000°C along ⟨100⟩. After [30]

$$\tau_f = \gamma / b \qquad (1)$$

where γ is the APB or stacking fault energy, and b, the absolute value of the Burgers vector. In this paper, t_2 denotes the variant in which the frictional stress appears, and t_1, the variant where the matrix dislocations are perfect dislocations and do not trail planar defects.

The following discussion in terms of very simple line tension agruments is based on the models described in [4–6] and arrives at essentially the same conclusions. In addition to Eq. (1) only one other formula is necessary for the discussion, the relation between the radius of curvature R of a bowed-out dislocation segment and the stress τ causing the bowing

$$R = \Gamma / (\tau b) \qquad (2)$$

Here, $\Gamma = 3.5 \times 10^{-9}$ N is the line tension of dislocations calculated for the simple case of isotropic line tension (the radius of curvature is independent of the dislocation character). The average of the line energies of screw and edge dislocations is used for Γ, $\Gamma = K b^2/(4\ \pi)\ \ln\ (l/(5\ r_o))$, with $K = 89.1$ GPa being the

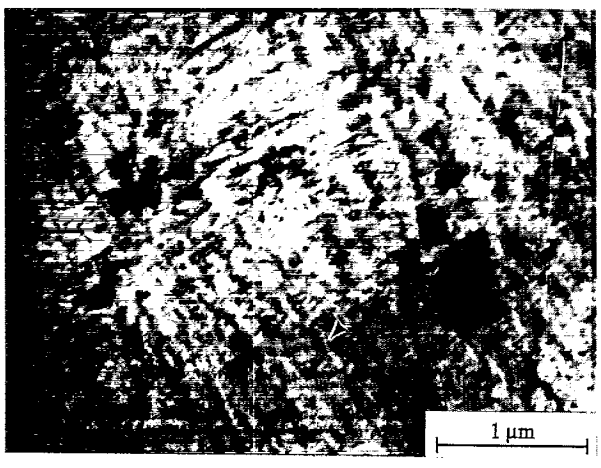

Fig. 10. Dislocations bowing out during in situ deformation in the HVEM of t′ zirconia at 1150°C

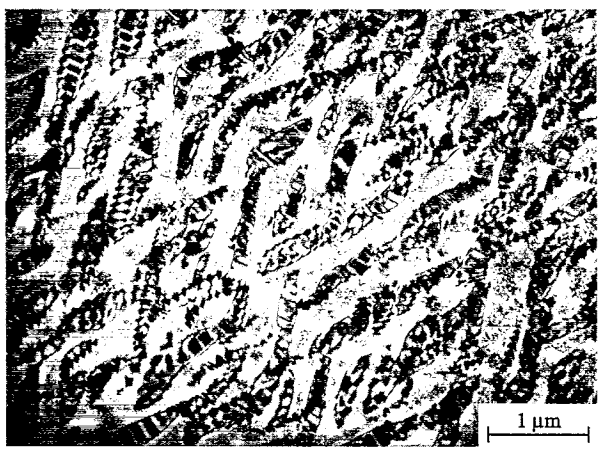

Fig. 11. Microstructure of partially stabilized zirconia (5.5 mol% Y_2O_3) showing twinned tetragonal colonies in a cubic matrix

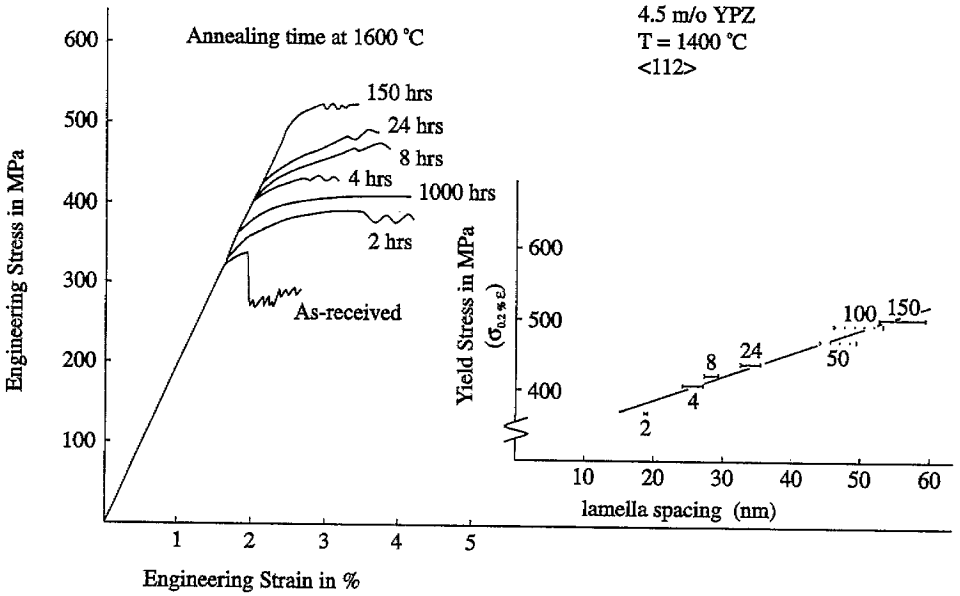

Fig. 12. Precipitation hardening of PSZ single crystals. Dependence of stress-strain curves at 1400°C on annealing time at 1600°C and dependence of yield stress on lamella spacing (inset). The numbers at the data points indicate the annealing time in h. After [4,6].

average value of the elastic energy factors of screw and edge dislocations taken from Table 3 of [20], $l = 70$ nm, the width of the lamellae, and $r_o = b = 0.367$ nm, the inner cut-off radius.

As a first step, the the peak-aged condition is discussed, i.e. after 150 h annealing at 1600°C. The flow stress at 1400°C is 550 MPa corresponding to a resolved shear stress $\tau_y = 550$ MPa $\times$ 0.47 $\cong$ 260 MPa (0.47 is the orientation factor), the lamella spacing is about $d = 57$ nm [4], the diameter of the precipitates, $D = 250$ nm, the length of the precipitates is 1.7 μm, and the precipitate volume fraction, $f = 0.4$. The interaction force between the dislocation and the precipitates is highest if the precipitates cannot be cut, but have to be surpassed by the Orowan process. To determine the Orowan stress, the distance L between the precipitates has to be known. This width of the matrix channels can be roughly estimated by considering the precipitates as elongated fibres in parallel arrangement within a square array, as outlined in Fig. 13(b), which shows that the volume fraction of precipitates is given by $f = \pi(D/2)^2/(L + D)^2$, yielding

$$L = D([\pi/4f]^{1/2} - 1) \tag{3}$$

The usual assumption of spherical precipitates leads to a very similar result so that this formula is not very sensitive to the shape of precipitates. Using the above data for the peak-aged condition, the width of the matrix channels becomes $L = 100$ nm.

The simplest estimation of the Orowan stress is based on the assumption that the dislocations have to bow out between the particles to semicircles as shown in Fig. 13(c), i.e. the radius of curvature in the matrix is given by $R_m = L/2$. From Eq. (2) it follows

$$\tau_{y,or} = 2\,\Gamma/(L\,b) \tag{4}$$

With the data above, $\tau_{y,or} = 190$ MPa, which is somewhat smaller than the experimental flow stress of 260 MPa.

Overageing after longer annealing times can generally be explained by assuming that the volume fraction f does not increase further while the size of particles is still growing, leading to an increasing particle spacing L according to Eq. (3). In the particular material, however, the width of the tetragonal domains d displayed in the inset of Fig. 12 is of the same order of magnitude as that of the matrix channels. It has experimentally been observed [5] that the dislocations can enter every second domain in the overaged state. It may therefore be concluded that in the peak-aged state the width of the matrix channels becomes equal to that of the domains so that the dislocations can shear the particles at least in the domains denoted above by t_1. Fig. 13(a) shows the shape of the dislocation inside a precipitate for the case of cutting both types of lamellae, i.e. t_1 in which no APB-like defect has to be created and t_2, where a defect has to be trailed. The condition for the dislocation to enter only t_1 is met if the radius of curvature in t_1 is equal to half the domain width: $R_{t1} = d/2$. With

$$d/2 = R_{t1} = \Gamma/(\tau_y\,b) \tag{5}$$

see Eq. (2), the critical width for entering t_1 becomes $d = 72$ nm, which is in good agreement with the data of

Fig. 12. Supposing that the lamellae t_2 cannot be cut at the same stress yields a lower bound of the friction stress τ_f or the antiphase boundary energy γ in Eq. (1). Lamellae t_2 cannot be cut if $R_{t2} \leq d/2$. Considering that inside t_2 the dislocations are bowed backward and that the stress is the difference between the applied stress and the friction stress, Eq. (2) yields $R_{t2} = \Gamma/([\tau_f - \tau_y]b) = \Gamma/(\gamma - \tau_y b)$ or, in the peak-aged state

$$\gamma \geq 2\,\Gamma/d_{peak} + \tau_{y,peak}\,b \quad (6)$$

Inserting the respective data yields $\gamma \geq 0.19$ J m^{-2}, which is in agreement with the conclusions in [5]. This value is relatively high and should be characteristic of stacking faults or APB-like defects on cube planes. Under the conditions described, the dislocations create Orowan loops around the lamellae t_2. Experimentally, both situations have been observed, viz. dislocation loops around and inside the lamellae (the latter ones should be unstable), and dislocation segments cutting t_1 and t_2.

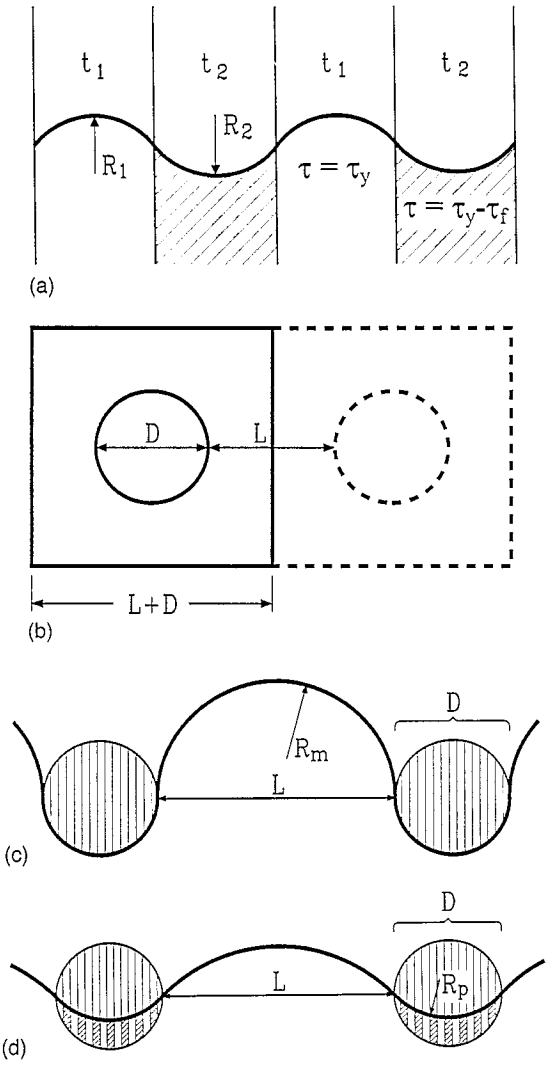

Fig. 13. Model of precipitation hardening in PSZ. (a) Precipitates cut by a dislocation forming APB-like defects in the t_2 lamellae. (b) Square array of precipitate fibres in the matrix. (c) Precipitates surrounded by a dislocation in the Orowan process. (d) Shape of dislocation when cutting small particles.

Cutting t_2 is possible for $R_{t2} \geq d/2$. On cutting the whole particle, the force balance of the line tensions along the boundary between t_1 and t_2 requires (if additional forces do not act at the boundary) $R_{t1} = R_{t2}$, as sketched in Fig. 13(a), resulting in

$$\tau_y = \tau_f/2 = \gamma/2\,b \quad (7)$$

Comparing this with Eq. (1) shows that the particles as a whole act like such of half the stacking fault energy in t_2. τ_y is the flow stress if $L < d$. If this condition is not met $\tau_{fp} = \gamma/2\,b$ represents the friction stress for particle cutting.

The present discussion of the peak-aged condition was based on the assumption that the matrix channels are not wider than the lamellae t_1, and that t_2 cannot be sheared. Increasing the lamellae width by further annealing will then decrease the flow stress according to Eq. (5), in agreement with the observed overageing. If the whole particles can be sheared Eq. (7) predicts the flow stress to be independent of the lamella spacing. For $R_{t2} = d/2$, Eq. (6) predicts $\gamma = 0.19$ J m^{-2}. At increasing spacing, however, the condition of $R_{t2} \leq d/2$ may be obtained so that Orowan looping around the t_2 lamellae may take place only at the later stages of ageing.

The early stages of ageing will now be treated. These stages are described in the usual terms of precipitation hardening, with the friction stress in the particles given by $\tau_{fp} = \gamma/2b$ and $L > d$. Small particles can be cut as long as the radius of curvature of the dislocation inside the particles is given by $R_p > D/2$, as sketched in Fig. 13(d) and by analogy with the individual lamellae above. R_p is given by

$$R_p = \Gamma/([\tau_{fp} - \tau_y]\,b) = \Gamma/(\gamma/2 - \tau_y\,b)$$

For small particles, $\tau_{fp} \gg \tau_y$, and consequently

$$R_p \cong 2\,\Gamma/\gamma \quad (8)$$

For $\gamma \geq 0.19$ J m^{-2} as estimated above, $R_p \leq 36$ nm, i.e. precipiates of a diameter smaller than a critical value of 72 nm, or smaller (since the value of γ is possibly a lower limit), can be sheared. In this case, the force balance at the particle interface $\tau_y bL = \gamma D/2$ yields

$$\tau_y = \gamma D/(2\,b\,L) \quad (9)$$

At this early stage of ageing, the yield stress strongly increases, by increasing D and decreasing L. If the critical diameter for the Orowan process is reached, i.e. for $D/2 > R_p \cong 2\,\Gamma/\gamma$, Eq. (4) applies, with τ_y increasing solely via a decreasing L, until peak-ageing when L becomes equal to d, as described above.

Fig. 14. Dislocations and planar faults in PSZ containg 6.8 mol% Y_2O_3 being annealed at 1600°C for 50 h and deformed at 1400°C. After [32].

The models outlined explain a strong precipitation hardening at the early stages with the precipitates being cut, a more moderate hardening during the later stages with Orowan loops being created around the precipitates, peak-ageing being reached when the width of the matrix channels becomes equal to the lamellae spacing, and finally overageing when the t_1 lamellae become wide enough for matrix dislocations to penetrate.

5.3. Other experimental observations

A block of ZrO_2 of a nominal concentration of 5.7 mol% of Y_2O_3 was annealed at 1600°C for 50 h, which should result in the equilibrium concentration of tetragonal precipitates. Owing to spatial variations of the yttria concentration, different microstructures were produced in different regions of the sample as e.g. the large precipitate fibres imaged in Fig. 11 in a region of 5.5 mol% Y_2O_3. In other regions, the yttria concentration was higher. At 1400°C a deformation experiment was carried out along a ⟨102] compression axis on a sample of 6.8 mol% Y_2O_3 [35]. At this compression axis, the orientation factors for slip on cube planes and on {101] planes, respectively, are almost equal. This sample had a very low yield stress of only 160 MPa corresponding to a critical shear stress of only about 60 MPa on both types of planes. A transmission electron microscope study in the HVEM revealed that the precipitates were very fine, in agreement with the high yttria concentration. As shown in Fig. 14, the dislocations are partial dislocations trailing planar defects. A detailed analysis revealed that the matrix is not cubic as expected from the phase diagram, that the Burgers vectors of the dislocations have ⟨101] directions, and that the planar defects show APB-like contrast and are arranged on {101] planes. This is probably the first direct evidence that partial dislocations in tetragonal zirconia trail the APB-like defects. The question arises why these faults are not arranged on cube planes which are the planes of lowest glide resistance in cubic zirconia. A qualitative answer can be obtained by analysing the arrangement of ions sketched in Fig. 15. Fig. 15(a) presents a view on a cube plane at the level of the oxygen ions, drawn as circles. Their shift in the tetragonal structure is exaggerated and additionally indicated by arrows. Fig. 15b shows the following layer of oxygen ions having reverse shifts. Superimposing Fig. 15(b) on Fig. 15(a) reveals the correct stacking sequence with rows of oxygen ions alternately shifted upwards and downwards. The motion of a partial dislocation of a 1/2 ⟨101] Burgers vector on a {010) plane corresponds to a displacement of the upper layer by the vector indicated by arrows in Fig. 15(a). As a result, whole rows of oxygen ions shifted in the same direction are arranged on top of each other, certainly representing a fault of high energy. This is the structure of the faults which in Section 5.2 are discussed as the origin of precipitation hardening for cube slip in PSZ, having an energy $\gamma_{\{100\}} \geq 0.19\ \mathrm{J\ m^{-2}}$. On the other hand, slip of a partial dislocation on a {101) plane creates a fault as outlined in Fig. 15(c). In this case, pairs of reduced distance between the oxygen ions always alternate with pairs of increased distance. They alternate along the trace of the slip plane in the image plane as well as perpendicular to it. Most probably, the energy of these faults is far lower than that on cube planes. An upper bound of this energy can be calculated from Eq. (1) by setting $\tau_f = \tau_y$ assuming that no other process contributes to the flow stress. With $\tau_y \cong 60$ MPa quoted above, this yields $\gamma_{\{101\}} \cong 0.02\ \mathrm{J\ m^{-2}}$. With this APB energy, the width of a superdislocation should be of the order of magnitude of 100 nm. In the experiment (Fig. 14), however, the partial dislocations seem to move independently, indicating that the stacking fault energy is certainly considerably lower than $0.02\ \mathrm{J\ m^{-2}}$. For comparison, the width of a superdislocation on a cube plane should be of the order of magnitude of 10 nm. These superdislocations have never been observed. Nevertheless, the APB energy in tetragonal zirconia on {101) planes seems to be more than one order of magnitude lower than that on {100) planes. The experiment described allows two conclusions. First, the matrix in PSZ crystals may be tetragonal instead of cubic and, second, partial dislocations in the tetragonal structures may move preferentially on {101) planes.

Some specimens of the same block had a slightly lower yttria concentration (6.6 mol%). Macroscopic compression experiments at 1400°C [31] yielded different yield stresses of 310 MPa on an average. This relatively low value fits the tendency observed in [6] of the flow stress to decrease at yttria concentrations close

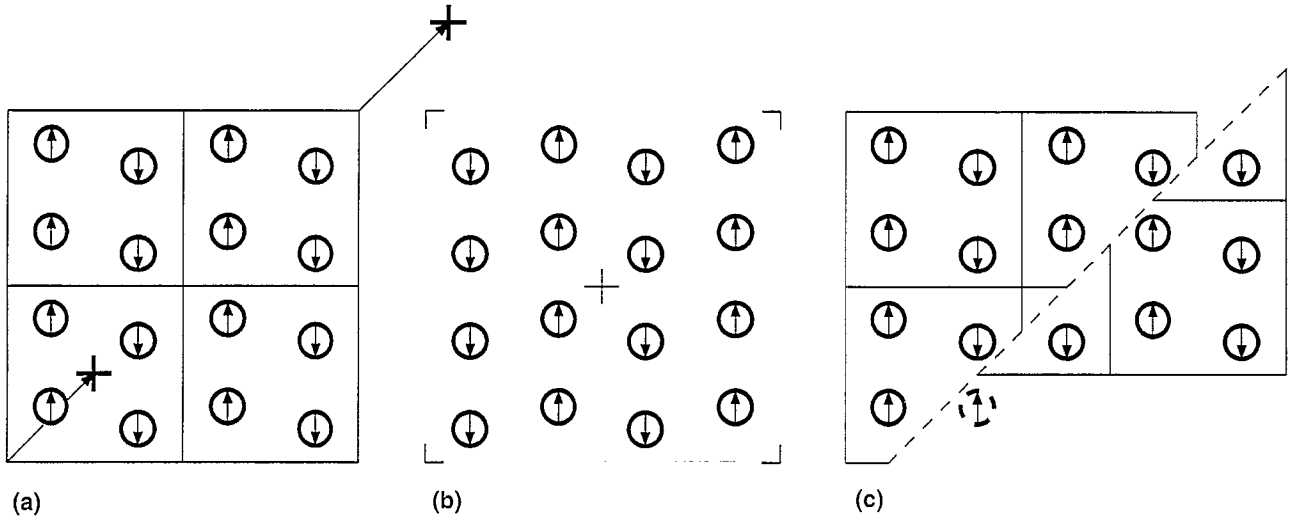

Fig. 15. Structure of planar faults on {100} and {101} slip planes.

to the cubic phase field. The strain rate sensitivity of the flow stress amounted to about 4 MPa on an average. Other data on the strain rate sensitivity have not been quoted in the literature. The low value corresponds to the athermal behaviour observed in cubic zirconia around 1150°C and in the kinetic dislocation behaviour at 1400°C. In cubic zirconia, however, the deformation is controlled by recovery at low strain rates. Thus, one important difference between cubic and partially stabilised zirconia may be that recovery is suppressed in the latter. Unfortunately, no data are available on the dislocation densities and mutual arrangements in PSZ which allow an estimation of the contribution of work-hardening to the flow stress. In [5], work-hardening in a particle-strenghtened material is one interpretation to explain the high strength of PSZ.

In situ straining experiments in the HVEM were performed on the same material at 1150°C [37]. The size of the precipitates shows a bimodal distribution: few large colonies coexist with a great number of very fine precipitates, forming the so-called tweed structure. Both consist of twinned domains on different size scales. The outstanding feature observed in the in situ experiments is the disappearance of the strong electron microscopy contrast of the twinned precipitates during loading on the analogy of the ferroelastic deformation of t′ zirconia, described in Section 4. For the large colonies, the contrast of individual domains disappears instantaneously whereas in the tweed structure, a boundary between the dark untransformed areas and the bright transformed ones is continuously shifting. Fig. 16 shows the microstructure after partial transformation. Of the large colonies at the centre, the cores of two precipitates appear very bright with their outer parts, however, still exhibiting the untransfomed domain structure. In the surrounding tweed structure, the darker untransformed regions can well be distinguished from the areas already transformed. Electron diffraction reveals the matrix of this material to be again tetragonal and the crystals most probably tetragonal single crystals after loading, as in t′ zirconia. The total macroscopic strain of the ferroelastic deformation should, however, be small (about 1% times the volume fraction of the precipitates of perhaps 20%) so that this effect will be very difficult to observe in macroscopic tests. On the other hand, ferroelastic deformation should severely affect the dislocation plasticity as it changes the defect structure of the crystals.

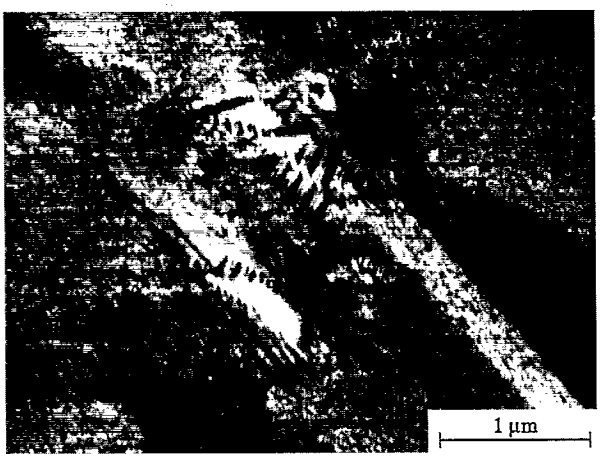

Fig. 16. Precipitate colonies and tweed structure in PSZ containg 6.6 mol% Y_2O_3 being annealed at 1600°C for 50 h. The structure has partly undergone ferroelastic deformation during in situ straining in an HVEM at 1150°C. [100] tensile direction and [01 $\bar{1}$] foil normal.

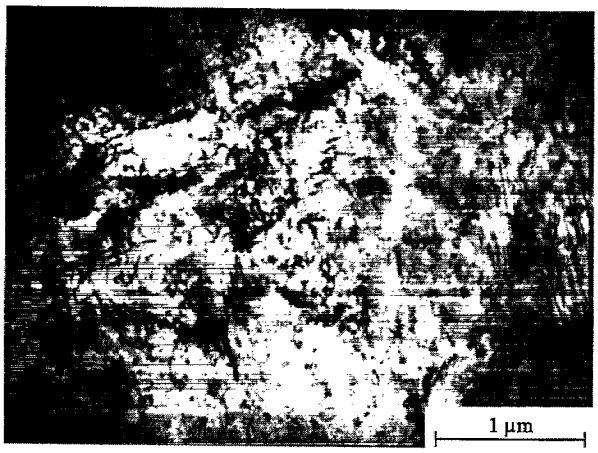

Fig. 17. Dislocations introduced in PSZ by in situ straining as in Fig. 16

During ferroelastic deformation, dislocations are rarely observed. They are generated, however, on further loading as shown in Fig. 17. Their density is highest in the regions of the formerly large colonies, e.g. in the middle of the figure, where the dislocations are quite straight. Both findings suggest that the dislocations move quite easily in the tetragonal single crystals. In the tweed structure, the dislocations are of curly shape owing to their interaction with the small precipitates. Many dislocation loops have formed. The small ones could be the Orowan loops around precipitates. If the precipitates really have undergone ferroelastic deformation prior to the dislocation motion and if the material represents a tetragonal single crystal, the interaction with the dislocations cannot be controlled by the processes described in Section 5.2. The pinning may be caused by the APB-like defects left behind after transformation. A similar open question about the effective obstacles already arose in the discussion of the dislocation motion in t′ zirconia. Larger dislocation loops of about 100 nm in diameter have certainly formed by the double cross slip process in connection with dislocation multiplication, as in cubic zirconia.

Concluding this section, it may be said that PSZ crystals often seem to have a tetragonal matrix in contrast to the prediction of the phase diagram. The tetragonal precipitates may undergo ferroelastic deformation so that in tension the crystal becomes a tetragonal single crystal containing residual APB-like defects at the boundaries of the former colonies or precipitates, respectively. Dislocations seem to easily move in the tetragonal single crystal, partial dislocations preferably on {101} planes where the APB energy is low. The residual defects seem to be strong obstacles. The microstructure prevents extended recovery, which is the origin of the soft behaviour of cubic zirconia at the same temperature.

6. Conclusions and open questions

Zirconia crystals exhibit very different microstructures causing different mechanical behaviour at high temperatures, depending on the concentration of the stabilizing yttria and on the annealing treatment.

Cubic zirconia shows textbook behaviour of dislocation plasticity. In the different temperature ranges, the deformation is controlled by the lattice resistance at low temperatures, and by localized obstacles or jogs at increased temperature. At about 1150°C the deformation behaviour becomes athermal and can be understood by long-range interactions between parallel dislocations and by the back stress of dislocations bowing out between large jogs. In the high-temperature range, recovery controls the flow stress, particularly at low strain rates. This relatively well-characterized behaviour refers to slip on cube planes. In spite of detailed microstructural evidence, it cannot be decided whether below about 900°C the dislocations are locally pinned by precipitates or jogs. The dislocation behaviour on non-cube planes is far less well understood. At low temperatures, the critical flow stress on these systems is probably very high. In the athermal region of cube slip, some kind of lattice friction seems to be responsible for the higher resolved flow stress for glide on non-cube planes. At increasing temperatures, the differences between cube and non-cube slip gradually disappear. The influence of the yttria concentration on the flow stress is well documented in the high-temperature range. However, there are almost no respective measurements for the lower temperature ranges.

t′ zirconia consists of individual domains with their c-axes in different orientations. Domains of alternating directions of the c-axes are stacked to form colonies elongated in ⟨111⟩ directions, filling the whole crystal volume in a characteristic way. In t′ zirconia, ferroelastic domain switching precedes dislocation plasticity. In tension, it results in a tetragonal single crystal containing residual defects. The coercive stress seems to strongly depend on temperature and to lie between the yield stresses of cubic and well annealed partially stabilized zirconia. During plastic deformation, the dislocations strongly bow out. The defects causing the bowing are not known.

Partially stabilized zirconia contains tetragonal precipitates with an internal structure similar to the colonies in t′ zirconia. According to the phase diagram, the matrix should be of cubic structure. In several cases, however, the matrix turned out to be tetragonal. Strong precipitation hardening of partially stabilized zirconia can be understood if complete dislocations in the matrix have to form APB-like defects in part of the tetragonal variants inside the precipitates. The energy

of these defects seems to be high (≥ 0.19 J m^{-2}) for cube slip, but very low (≤ 0.02 J m^{-2}) for slip on {101} planes. The details of this process depend on the width of both the matrix channels as well as the individual domains, which both change during ageing. In situ straining experiments on yttria-rich PSZ inside an HVEM have shown that ferroelastic domain switching can take place also in PSZ, removing the original domain structure before dislocation plasticity starts. It is not clear whether or not the domain switching is restricted to only a few types of PSZ. In this context, the question of the origin of the hardening effect is open. It may either be the trailing of the APB-like defects by partial dislocations in the tetragonal structure, or the interaction with the residual defects at the precipitate boundaries. Anyway, the particular microstructure of PSZ prevents recovery, which plays an essential role in the high-temperature deformation of cubic zirconia.

Up to now, macroscopic experiments on PSZ have been carried out at 1400°C only. Thus, nothing is known about the temperature dependence of the hardening mechanism. Besides, owing to the difficulty of imaging dislocations in the domain structure, Burgers vectors have been determined in only very few cases so that it is open whether the majority of dislocations are partial or complete ones. Except [35], there is no evidence that APB-like defects are generated by moving partial dislocations. Besides, only very limited information exists on the activated slip planes. Cube slip is concluded from macroscopic slip traces on specimens loaded along ⟨112⟩ whereas {110} slip planes were observed after loading along ⟨100⟩. The great difference probably occurring between the APB energies on cube and {110} planes suggests that the latter ones should be the preferred planes for individual partial dislocations to move. Thus, inspite of detailed models available of precipitation hardening in PSZ, serious basic questions are still open concerning the dislocation motion in this material.

Acknowledgements

The authors wish to thank Professors Arthur H. Heuer and Manfred Rühle for many stimulating discussions. Financial support by the Deutsche Forschungsgemeinschaft is gratefully acknowledged for the work accomplished in Halle.

References

[1] A.H. Heuer, J. Am. Ceram. Soc. 70 (1987) 689.
[2] D.J. Green, R.H.J. Hannink, M.W. Swain, Transformation Toughening of Ceramics, CRC Press, Boca Raton, Fla, 1989.
[3] A. Dominguez-Rodriguez, V. Lanteri, A.H. Heuer, J. Am. Ceram. Soc. 69 (1986) 285.
[4] A.H. Heuer, V. Lanteri, A. Dominguez-Rodriguez, Acta Metall. 37 (1989) 559.
[5] J. Martinez-Fernandez, M. Jimenez-Melendo, A. Dominguez-Rodriguez, K.P.D. Lagerlöf, A.H. Heuer, Acta Metall. Mater. 41 (1993) 3171.
[6] J. Martinez-Fernandez, M. Jimenez-Melendo, A. Dominguez-Rodriguez, P. Cordier, K.P.D. Lagerlöf, A.H. Heuer, Acta Metall. Mater. 43 (1995) 2469.
[7] A. Virkar, R. Matsumoto, J. Am. Ceram. Soc. 69 (1986) C224.
[8] C.-J. Chan, F.F. Lange, M. Rühle, J.-F. Jue, A.V. Virkar, J. Am. Ceram. Soc. 74 (1991) 807.
[9] K.M. Prettyman, J.-F. Jue, A.V. Virkar, C.R. Hubbard, O.B. Cavin, M.K. Ferber, J. Mater. Sci. 27 (1992) 4167.
[10] A.H. Heuer, R. Chaim, V. Lanteri, in: S. Somiya, N. Yamamoto, H. Hanagida (Eds.), Advances in Ceramics, vol. 24, Science and Technology of Zirconia III, Am. Ceram. Soc., Westerville OH, 1988, p. 3.
[11] H.G. Scott, J. Mater. Sci. 10 (1975) 1527.
[12] V.S. Stubican, in: S. Somiya, N. Yamamoto, H. Hanagida (Eds.), Advances in Ceramics, vol. 24, Science and Technology of Zirconia III, Am. Ceram. Soc., Westerville OH, 1988, p. 71.
[13] J. Martinez-Fernandez, M. Jimenez-Melendo, A. Dominguez-Rodriguez, Acta Metall. Mater. 43 (1995) 593.
[14] D.S. Cheong, A. Dominguez-Rodriguez, A.H. Heuer, Philos. Mag. A 60 (1989) 123.
[15] D.S. Cheong, A. Dominguez-Rodriguez, A.H. Heuer, Philos. Mag. A 63 (1991) 377.
[16] A. Dominguez-Rodriguez, D.S. Cheong, A.H. Heuer, Philos. Mag. A 64 (1991) 923.
[17] D. Goméz-Garcia, J. Martinez-Fernández, A. Dominguez-Rodriguez, P. Eveno, J. Castaing, Acta Mater. 44 (1996) 991.
[18] B. Baufeld, M. Bartsch, U. Messerschmidt, D. Baither, Acta Metall. Mater. 43 (1995) 1925.
[19] B. Baufeld, Doctoral Thesis, Martin Luher University Halle/Saale, Germany, 1996.
[20] U. Messerschmidt, B. Baufeld, D. Baither, in: E. Kisi (Ed.), Zirconia Engineering Ceramics: Old Challenges-New Ideas, Key Eng. Mater., Trans. Tech. Publ., in press.
[21] D. Baither, B. Baufeld, U. Messerschmidt, M. Bartsch, Mater. Sci. Eng. A, 233 (1997) 75.
[22] B. Ya. Farber, A.S. Chiarelli, A.H. Heuer, Philos. Mag. A 72 (1995) 59.
[23] U. Messerschmidt, B. Baufeld, K.J. McClellan, A.H. Heuer, Acta Metall. Mater. 43 (1995) 1917.
[24] U.F. Kocks, Physical Basis for Non-Elastic Constitutive Relations, Discussion paper at Symp. Adv. in Metal Deformation, Cornell University, Ithaca, NY, 1976.
[25] F.R. Chien, A.H. Heuer, Philos. Mag. A 73 (1996) 681.
[26] D. Baither, B. Baufeld, U. Messerschmidt, A. Foitzik, M. Rühle, J. Am. Ceram. Soc., in press.
[27] B. Baufeld, U. Messerschmidt, D. Baither, M. Bartsch, A. Foitzik, M. Rühle, in: R.C. Bradt, C.A. Brooks, J. Routbort. (Eds.), Plastic Deformation of Ceramics, Plenum Press, NY, 1995, p. 43.
[28] U. Messerschmidt, B. Baufeld, D. Baither, M. Bartsch, Proc. 4th Euroceramics Conf., Riccione, Italy, October 2–6, 1995, Gruppo Editoriale Faenza, Faenza, 1995, p. 479.
[29] D. Baither, B. Baufeld, U. Messerschmidt, M. Bartsch, A. Foitzik, M. Rühle, J. Am. Ceram. Soc., in press.
[30] A. Foitzik, M. Stadtwald-Klenke, M. Rühle, Z. Metallkunde 84 (1993) 397.

[31] B. Baufeld, D. Baither, U. Messerschmidt, unpublished results
[32] M.G. Cain, S.M. Bennington, M.H. Lewis, S. Hull, Philos. Mag. B69 (1994) 499.
[33] A. Dominguez-Rodriguez, A.H. Heuer, Crystal Lattice Def. Amorphous Mater. 16 (1987) 117.
[34] P. Teracher, Doctoral Thesis, University Poitiers, 1990
[35] D. Baither, B. Baufeld, U. Messerschmidt, J. Am. Ceram. Soc. 78 (1995) 1375.
[36] D. Baither, B. Baufeld, U. Messerschmidt, Phys. Status Solidi A 137 (1993) 569.
[37] B. Baufeld, D. Baither, U. Messerschmidt, M. Bartsch, Phys. Status Solidi A 150 (1995) 297.